



Article

Finite-Time Path-Following Control of Underactuated AUVs with Actuator Limits Using Disturbance Observer-Based Backstepping Control

MohammadReza Ebrahimpour ¹  and Mihai Lungu ^{2,*} 

¹ Faculty of Electrical and Computer Engineering, Tarbiat Modares University, Tehran 1411713116, Iran; m.ebrahimpour11@gmail.com

² Faculty of Electrical Engineering, University of Craiova, 200585 Craiova, Romania

* Correspondence: lma1312@yahoo.com

Abstract: This paper presents a three-dimensional (3D) robust adaptive finite-time path-following controller for underactuated Autonomous Underwater Vehicles (AUVs), addressing model uncertainties, external disturbances, and actuator magnitude and rate saturations. A path-following error system is built in a path frame using the virtual guidance method. The proposed cascaded closed-loop control scheme can be described in two separate steps: (1) A kinematic law based on a finite-time backstepping control (FTBSC) is introduced to transform the 3D path-following position errors into the command velocities; (2) The actual control inputs are designed in the dynamic controller using an adaptive fixed-time disturbance observer (AFTDO)-based FTBSC to stabilize the velocity tracking errors. Moreover, the adverse effects of magnitude and rate saturations are reduced by an auxiliary compensation system. A Lyapunov-based stability analysis proves that the path-following errors converge to an arbitrarily small region around zero within a finite time. Comparative simulations illustrate the effectiveness and robustness of the proposed controller.

Keywords: path-following; backstepping control; sliding mode control; disturbance observer; finite-time control; fixed-time control



Academic Editors: Jimin Hwang,
Neil Bose and Shuangshuang Fan

Received: 11 December 2024

Revised: 12 January 2025

Accepted: 14 January 2025

Published: 18 January 2025

Citation: Ebrahimpour, M.; Lungu, M. Finite-Time Path-Following Control of Underactuated AUVs with Actuator Limits Using Disturbance Observer-Based Backstepping Control. *Drones* **2025**, *9*, 70. <https://doi.org/10.3390/drones9010070>

Copyright: © 2025 by the authors. Licensee MDPI, Basel, Switzerland. This article is an open access article distributed under the terms and conditions of the Creative Commons Attribution (CC BY) license (<https://creativecommons.org/licenses/by/4.0/>).

1. Introduction

AUVs can explore underwater environments and perform various applications such as pipeline inspection, military missions, oceanography, etc. [1]. Problems such as highly nonlinear and coupled dynamics, uncertain hydrodynamic parameters, and unknown exogenous disturbances are serious obstacles to the precise control of submarines. Furthermore, due to weight, cost, reliability, and energy consumption considerations, most AUVs have underactuated structures, i.e., they lack control inputs for their lateral and vertical movements. Maneuverability and disturbance rejection properties are reduced due to non-integrable second-order non-holonomic constraints in underactuated systems [2]. The literature presents various path-following and trajectory-tracking techniques, which are the basis of various motion controllers for underwater vehicles. The main goal of a trajectory-tracking controller is to guide an AUV to reach a specific position at a predetermined point in time, while there is no time constraint on the path-following task and only the geometry of the target path is important. In general, path-following methods have the potential to exhibit smoother convergence properties and the probability of control inputs

reaching saturation limits is lower compared to trajectory-tracking controllers [3]. Therefore, considering the above issues, focusing on the study and design of the path-following control methods for underactuated AUVs can improve their practical capabilities.

1.1. Antecedents and Motivations

One of the most powerful control techniques in the design of nonlinear motion controllers for underactuated AUVs is the backstepping control (BSC) [4]. Since the hydrodynamic effects acting on an AUV vary significantly with the working and environmental conditions [5], it is difficult to accurately measure and estimate model parameters and exogenous disturbances. This issue degrades the performance of the conventional BSC-based methods in practical implementation. To handle this problem, the BSC-based schemes, equipped with observers or combined with more robust control methods, have been widely applied to AUV motion control [6–8]. In [9], a nonlinear adaptive disturbance observer (DO) employing the high-order sliding mode control (SMC) method is designed to improve the anti-disturbance characteristics of a backstepping-based trajectory-tracking controller. In [10], a double-loop backstepping sliding mode controller is designed for underactuated AUVs. A nonlinear DO is employed in the inner loop to cope with the model's uncertainties and linearization errors. In [11], an adaptive asymptotic control law is incorporated into a design based on BSC to compensate for non-vanishing uncertainties. In [12], a combination of BSC and SMC is applied to make an underactuated AUV follow a target path, a fuzzy logic (FL)-based adaptive law handling the parameter and environmental disturbances. In [13], a control scheme based on BSC is proposed for path-following tasks, where an extended state observer (ESO) is developed to estimate the mismatched lumped disturbance and recover the unmeasured velocities.

It is also worth mentioning the various strong points of the SMC-based approaches for underactuated AUVs. The main drawback of the control strategies based on SMC is the “chattering phenomenon” [6], its direct effect being related to the low control performance and high wear of actuators. Also, the bounds of uncertainties must be completely known to ensure stability, which is not feasible in practice. Designing higher-order sliding manifolds [14,15], DO-based SMC [16–18], and adaptive SMC [15,19] are some techniques to alleviate these drawbacks. In [20], a neural network (NN) and an FL-based adaptive term are applied to deal with the unknown exogenous disturbances, parameter uncertainties, and the chattering in SMC. In [15], an adaptive twisting SMC is designed for the trajectory tracking task that can handle the chattering effect and prior knowledge problem. In [21], an adaptive trajectory-tracking scheme based on SMC with prescribed performance is designed, where an NN is employed to compensate for the effects of external time-varying disturbances and model uncertainties. In [22], a two-layer path-following controller for underactuated AUVs is developed, where the kinematic controller is based on BSC, and the dynamic control law is designed using a nonlinear DO and the integral SMC.

It is desirable that the path-following errors quickly reach the origin. However, the conventional control schemes can only ensure asymptotic stability [23,24], i.e., the tracking errors converge to the equilibrium point in infinite time. The methods with finite-time stability can reduce the settling time of tracking errors relative to the asymptotic controllers. However, the convergence time of the conventional finite-time controllers may be prolonged for large initial errors. Therefore, it seems that these controllers are not very suitable for applications where the initial conditions are not known in advance. This shortcoming can be partially overcome by using fast finite-time methods. In [25], a double-loop controller is introduced for path-following of underactuated AUVs, where global asymptotic stability of the position errors in the kinematic layer and finite-time convergence of the attitude tracking/surge velocity regulation errors in the dynamic layer are assured. In [26], a finite-

time terminal sliding mode control (TSMC) with a finite-time NN-based DO is employed in the dynamic layer of a 3D trajectory-tracking controller. In [27], a finite-time robust adaptive control based on a continuous TSMC method is proposed for trajectory-tracking tasks. In [28], a global finite-time trajectory-tracking control based on the dynamic surface control approach is designed, where a finite-time NN estimates the lumped uncertainties. In [29], an adaptive finite-time double-loop integral terminal sliding mode control (ITSMC) method is proposed for the trajectory-tracking control of AUVs, where a finite-time NN estimates the lumped uncertainty. In [30], a finite-time control method is proposed for trajectory-tracking of an over-actuated AUV using the non-singular fast TSMC equipped with an adaptive finite-time ESO. The problem of long convergence time for large initial errors can be completely overcome by fixed-time control methods; the upper bound of the convergence time of state trajectories depends only on the control parameters and not on the initial conditions. In [16], a DO-based BSC is integrated with a fixed-time control method to achieve fixed-time convergence considering environmental disturbances. In [31], a fixed-time control method is proposed for trajectory-tracking of underactuated AUVs, where an adaptive fixed-time DO is designed to compensate for ocean currents within a fixed time. In [32], a fixed-time controller based on SMC with DO is designed for the trajectory-tracking control problem of AUVs under time-varying external disturbances.

Control inputs for practical applications are confined by actuators' maximum producible forces/moments. Ignoring the physical limitations of the actuators' magnitude and rate in the control design can degrade control performance or even cause instability of the controlled system, especially when disturbances or mission maneuver requirements cause the inputs to greatly exceed their maximum capabilities [33]. Auxiliary compensation systems are usually employed to counteract the input magnitude saturation [5,6,21]. Also, actuator dynamics has been considered in some studies [33,34]. However, hard limits on input rate have not been taken into account in these investigations.

1.2. Main Contribution

This paper introduces a robust adaptive finite-time path-following controller for an underactuated AUV maneuvering in 3D space subject to parameter uncertainties, ocean currents, and actuator limits. The highlights of this study are as follows:

1. Different from the existing DOs introduced in [10,13,16,31,32,35], a continuous adaptive fixed-time integral sliding mode disturbance observer is designed to estimate the lumped disturbances with an arbitrarily bounded error in a fixed time. An adaptive law in the developed observer obtains an upper bound of uncertainty rate and eliminates the need for prior knowledge about uncertainties. The signum function in the observer is replaced by the hyperbolic tangent function and the approximation error is taken into account.
2. Compared to the finite-time control methods presented in [25–29], a novel finite-time control law based on the hyperbolic tangent function is developed; it ensures the path-following errors converge to a bounded region around the origin within a finite time. In addition, the proposed finite-time control law can better deal with the effect of time-varying disturbances, also providing smoother control inputs.
3. In contrast to the anti-saturation methods proposed in [5,6,21,24,33,34], both the magnitude and rate saturations are considered, an auxiliary compensation system being designed to maintain stability in the presence of control inputs with high changing rates.

The remainder of this paper is organized as follows: preliminaries and a problem statement, including the underactuated AUV dynamics and path-following error system, are given in Section 2. The designing procedure of the control scheme is described in

Section 3. The stability analysis of the introduced control law is performed through the Lyapunov theory in Section 4. The fifth part of this work contains a comparative simulation study. Finally, concluding remarks are presented in Section 6.

2. Preliminaries and Problem Statement

2.1. Preliminaries

Notations. In this paper, for any variable $x \in \mathfrak{R}$, the function $\text{sig}^a(x)$ is defined as $\text{sig}^a(x) = |x|^a \text{sign}(x)$, where a is a strictly positive parameter, $|\cdot|$ stands for the absolute value of a variable, and $\text{sign}(\cdot)$ indicates the signum function.

Consider the following nonlinear system:

$$\dot{\mathbf{x}} = \mathbf{f}(\mathbf{x}(t)), \mathbf{x}(0) = \mathbf{x}_0 \quad (1)$$

where $\mathbf{x} = [x_1, x_2, \dots, x_n]^T \in \mathfrak{R}^n$ and $\mathbf{f}: \mathcal{D} \rightarrow \mathfrak{R}^n$ is continuous on an open set $\mathcal{D} \subseteq \mathfrak{R}^n$ around zero.

Lemma 1 [31]. For any variable $x \in \mathfrak{R}_{>0}$ and constant $\lambda > 0$, the following expression holds:

$$0 < x(\text{sign}(x) - \tanh(\lambda x)) \leq \frac{l}{\lambda}, l = 0.2785 \quad (2)$$

Lemma 2 [36]. For the system (1), let $V(x): \mathfrak{R}^n \rightarrow \mathfrak{R}_{>0}$ be a positive definite and continuous function on $\mathcal{D} \subset \mathfrak{R}^n$ satisfying $\dot{V}(x) \leq -KV^a(x) + \Delta$ for $a \in (0, 1)$, $K > 0$, and $0 < \Delta < \infty$. Therefore, the system is practically finite-time stable, i.e., there exists a region $\mathcal{D}_0 \subset \mathfrak{R}^n$ such that any state trajectory from an initial value $x_0 \in \mathcal{D}_0$ converges to the invariant set Ω within a finite time no greater than t_s given by:

$$\Omega = \left\{ x \mid V^a(x) \leq \frac{\Delta}{K(1-\eta)} \right\}, t_s \leq \frac{V^{1-a}(x_0)}{K\eta(1-a)} \quad (3)$$

where $0 < \eta < 1$ is a parameter that specifies the size of the invariant set Ω .

Lemma 3 [37]. Let $V(x)$ be a positive definite and continuous function on $\mathcal{D} \subset \mathfrak{R}^n$ for the system (1) satisfying $\dot{V}(x) \leq -K_1V^a(x) - K_2V^b(x) + \Delta$, where K_1, K_2, a, b , and Δ are positive constants with $0 < a < 1$, $b > 1$, and $0 < \Delta < \infty$. Then, the system (1) is practically fixed-time stable, i.e., there exists a region $\mathcal{D}_0 \subseteq \mathfrak{R}^n$ such that any state trajectory from an initial value $x_0 \in \mathcal{D}_0$ converges to the invariant set Ω within a fixed time no greater than t_s given by:

$$\Omega = \left\{ x \mid V(x) \leq \min \left\{ \left(\frac{\Delta}{K_1(1-\eta)} \right)^{\frac{1}{a}}, \left(\frac{\Delta}{K_2(1-\eta)} \right)^{\frac{1}{b}} \right\} \right\}, t_s \leq \frac{1}{K_1\eta(1-a)} + \frac{1}{K_2\eta(b-1)} \quad (4)$$

where $0 < \eta < 1$.

Lemma 4 [38]. Consider the following dynamic system:

$$\dot{x}(t) = -k_1x(t) - k_2x^b(t) + \delta(t) \quad (5)$$

where $k_1 > 0$, $k_2 > 0$, and $b = \frac{2n+l}{2n+1} > 1$ are constants with $n, l \in \mathcal{N}$, and $\delta(t)$ is a positive function. Any state trajectory starting at a positive initial value remains positive for all times, i.e., $x(t_0) \geq 0 \Leftrightarrow x(t) \geq 0, \forall t \geq t_0$.

Lemma 5 [38]. *The following inequality is true for all variables x and y , and any constant a satisfying $y \geq 0$, $y - x \geq 0$, and $a > 1$.*

$$x(y - x)^a \leq \frac{a}{a + 1} (y^{a+1} - x^{a+1}) \tag{6}$$

Lemma 6 [38]. *The following inequality is satisfied for all variables $x, y \in \Re$ and constants $a, b, c \in \Re_{>0}$.*

$$|x|^a |y|^b \leq \frac{a}{a + b} c |x|^{a+b} + \frac{b}{a + b} c^{-\frac{a}{b}} |y|^{a+b} \tag{7}$$

Lemma 7 [37]. *The following inequalities hold for any variable $x_i \in \Re$, $i = 1, \dots, n$ and constants $0 < a < 1$ and $b > 1$:*

$$|x_i| \leq |x_i|^a + |x_i|^b \tag{8}$$

$$(|x_1| + |x_2| + \dots + |x_n|)^a \leq |x_1|^a + |x_2|^a + \dots + |x_n|^a \tag{9}$$

$$(|x_1| + |x_2| + \dots + |x_n|)^b \leq n^{b-1} (|x_1|^b + |x_2|^b + \dots + |x_n|^b) \tag{10}$$

2.2. AUV Dynamics

This subsection provides a brief introduction to the 3D dynamics of underactuated slender-body AUVs. The kinematic model associated with a vehicle moving in the 3D space is mainly defined by six motion variables related to the surge, sway, heave, roll, pitch, and yaw motions. For the control design in a slender-body AUV, the difference between the centers of gravity and buoyancy ensures a sufficient damping torque that can passively restore the roll motion, and hence, the roll dynamics can be neglected [2]. Moreover, some simplifying assumptions are usually considered in the dynamic modeling, such as: (i) the AUV’s center of mass (COM) coincides with the origin of the body-fixed frame $\{B\}$; (ii) the higher-order hydrodynamic drag terms have negligible values; (iii) the mass distribution is homogeneous.

The AUV’s kinematic equations are [2]:

$$\begin{cases} \dot{x} = u \cos \theta \cos \psi - v \sin \psi + w \sin \theta \cos \psi \\ \dot{y} = u \cos \theta \sin \psi + v \cos \psi + w \sin \theta \sin \psi \\ \dot{z} = -u \sin \theta + w \cos \theta \\ \dot{\theta} = q \\ \dot{\psi} = r / \cos \theta \end{cases} \tag{11}$$

with x , y , and z —coordinates of the origin of $\{B\}$ with respect to the Earth-fixed NED frame $\{E\}$, while θ and ψ denote the pitch and the yaw angles, respectively; these angles define the rotation matrix from $\{B\}$ to $\{E\}$; also, the AUV’s linear velocities and angular rates relative to $\{B\}$ are denoted by u , v , w , q , and r .

The AUV dynamic equations are [2]:

$$\begin{cases} m_{11} \dot{u} = m_{22} v r - m_{33} w q - f_{11} u + \tau_u - D_u \\ m_{22} \dot{v} = -m_{11} u r - f_{22} v - D_v \\ m_{33} \dot{w} = m_{11} u q - f_{33} w - D_w \\ m_{55} \dot{q} = (m_{33} - m_{11}) u w - f_{55} q - G h \sin \theta + \tau_q - D_q \\ m_{66} \dot{r} = (m_{11} - m_{22}) u v - f_{66} r + \tau_r - D_r \end{cases} \tag{12}$$

where τ_u denotes the control force generated by the propeller along the surge axis; τ_q and τ_r represent the control moments due to the rudders that are applied to produce proper angular motion around the y -axis and the z -axis of $\{B\}$, respectively; $D_{(\cdot)}$ are the environmental disturbances expressed in $\{B\}$; $f_{(\cdot)}$ represent hydrodynamic damping terms, $m_{(\cdot)}$ denote the combined inertia and added mass terms, and $h = z_g - z_b$, with z_g and z_b being the vertical coordinates associated with the centers of gravity and buoyancy, respectively.

The output and dynamics of the actuator are given by:

$$\begin{cases} \tau_v = \text{sat}(u_{a,v}) \\ \dot{u}_{a,v} = \text{sat}\left(\frac{1}{T_v}(u_{c,v} - u_{a,v})\right), v = u, q, r \end{cases} \quad (13)$$

where $u_{a,v}(0) = 0$ and T_v is the actuator time constant; $u_{a,v}$ denotes the actuator state and $u_{c,v}$ is the controller output; $\text{sat}(x) : \mathfrak{R} \rightarrow [x_{\min}, x_{\max}]$ represents the saturation function described by:

$$\text{sat}(x) = \begin{cases} x_{\max}, & x \geq x_{\max} \\ x, & x_{\min} < x < x_{\max} \\ x_{\min}, & x \leq x_{\min} \end{cases} \quad (14)$$

where x_{\max} and x_{\min} are the maximum and minimum limits of the saturation function, respectively.

Assumption 1. The AUV pitch angle is bounded by $|\theta| \leq \theta_{\max} < \frac{\pi}{2}$ to avoid singularities in (11).

Assumption 2. The system states used in the feedback control laws are all available through measurements by ideal sensors.

2.3. 3D Path-Following Error Dynamics

According to Figure 1, an AUV represented by point Q moves on a 3D path parameterized by a time-independent parameter $s \in \mathfrak{R}$. The path frame $\{F\}$ is attached to the virtual vehicle represented by point P , where the x -axis is along the tangent vector at point P , the y -axis of $\{F\}$ is parallel to the xy -plane of $\{E\}$, while the z -axis is chosen using the right-hand rule. We denote the inertial position and velocity vectors of the AUV's COM by $\mathbf{Q} = [x, y, z]^T$ and $\dot{\mathbf{Q}} = [\dot{x}, \dot{y}, \dot{z}]^T$, and those of the virtual vehicle on the path by $\mathbf{P} = [x_p(s), y_p(s), z_p(s)]^T$ and $\dot{\mathbf{P}} = [x'_p(s), y'_p(s), z'_p(s)]^T s$, respectively, with $x'_p(s) = \partial x_p / \partial s$, $y'_p(s) = \partial y_p / \partial s$, and $z'_p(s) = \partial z_p / \partial s$.

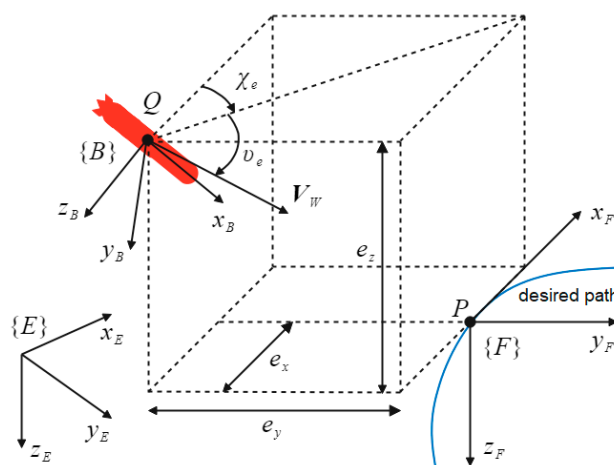


Figure 1. Diagram of the 3D path-following.

Consider the spatial error vector $\varepsilon = \vec{PQ}$ to define the path-following position errors expressed in $\{F\}$, as follows:

$$\varepsilon = [e_x, e_y, e_z]^T = \mathbf{R}_E^F(\mathbf{Q} - \mathbf{P}) \quad (15)$$

where e_x , e_y , and e_z denote the components of the path-following position error vector. \mathbf{R}_E^F denotes the rotation matrix from $\{E\}$ to $\{F\}$, defined by the course angles (the azimuth angle χ_P and the elevation angle v_P) of the virtual vehicle (point P):

$$\mathbf{R}_E^F = \begin{bmatrix} \cos \chi_P \cos v_P & \sin \chi_P \cos v_P & -\sin v_P \\ -\sin \chi_P & \cos \chi_P & 0 \\ \cos \chi_P \sin v_P & \sin \chi_P \sin v_P & \cos v_P \end{bmatrix} \quad (16)$$

with

$$\chi_P = \text{atan2}(y'_p(s), x'_p(s)), \quad v_P = \text{atan}\left(-z'_p(s) / \sqrt{x'_p(s)^2 + y'_p(s)^2}\right) \quad (17)$$

where the two-arguments function atan2 ensures that the mapping is confined by $(-\pi, \pi]$.

Taking the time derivative of ε , one obtains:

$$\dot{\varepsilon} = (\mathbf{S}_F)^T \mathbf{R}_E^F(\mathbf{Q} - \mathbf{P}) + \mathbf{R}_E^F(\dot{\mathbf{Q}} - \dot{\mathbf{P}}) \quad (18)$$

with

$$\mathbf{S}_F = \begin{bmatrix} 0 & -\dot{\chi}_P \cos v_P & \dot{v}_P \\ \dot{\chi}_P \cos v_P & 0 & \dot{\chi}_P \sin v_P \\ -\dot{v}_P & -\dot{\chi}_P \sin v_P & 0 \end{bmatrix} \quad (19)$$

We rewrite the third term in (18) as follows:

$$\mathbf{R}_E^F \dot{\mathbf{Q}} = \mathbf{R}_W^F \mathbf{V}_W \quad (20)$$

where $\mathbf{V}_W = [U, 0, 0]^T$, with $U = \sqrt{u^2 + v^2 + w^2}$, is the AUV's resultant velocity vector expressed in the flow frame $\{W\}$, and \mathbf{R}_W^F is the rotation matrix from $\{W\}$ to $\{F\}$:

$$\mathbf{R}_W^F = \begin{bmatrix} \cos \chi_e \cos v_e & -\sin \chi_e & \cos \chi_e \sin v_e \\ \sin \chi_e \cos v_e & \cos \chi_e & \sin \chi_e \sin v_e \\ -\sin v_e & 0 & \cos v_e \end{bmatrix} \quad (21)$$

where $\chi_e = \chi - \chi_P$ and $v_e = v - v_P$ are the yaw and pitch course-angle errors, with χ and v being the AUV's azimuth angle and elevation angle, respectively. The course-angle errors define the attitude deviation between the AUV's resultant velocity vector and the tangent vector at point P .

By replacing (15) and (20) into (18), we obtain the dynamics associated with the system of path-following error expressed relative to the $\{F\}$ frame:

$$\dot{\varepsilon} = (\mathbf{S}_F)^T \varepsilon + \mathbf{R}_W^F \mathbf{V}_W - \mathbf{V}_P \quad (22)$$

where $\mathbf{V}_P = \mathbf{R}_E^F \dot{\mathbf{P}} = [\dot{s}, 0, 0]^T$ is the velocity expression of the virtual vehicle in $\{F\}$.

2.4. Control Objectives

Starting from the dynamics of the AUV ((11) and (12)), let us define a continuously parameterized path to track with a reference profile for the surge velocity ($0 < u_d$). The feedback control laws expressing the thrusting force (τ_u), the pitch steering moment (τ_q), the yaw steering moment (τ_r), and the virtual vehicle's movement rate (\dot{s}) have to

be designed such that, despite the unknown environmental disturbances, the dynamic perturbations, and the actuators' limits, the off-track error $\|\epsilon\| = \sqrt{e_x^2 + e_y^2 + e_z^2}$ and the surge velocity tracking error ($e_u = u - u_d$) converge to arbitrarily small regions around zero within a finite time t_s , i.e.:

$$\lim_{t \rightarrow t_s} (\|\epsilon\|, |e_u|) \leq (\Delta_1, \Delta_2), t_s < \infty \tag{23}$$

where Δ_1 and Δ_2 are small positive constants.

3. Design of the Path-Following Controller

This section introduces a novel nonlinear robust adaptive cascaded control to make the AUV follow a reference path. Figure 2 depicts the block diagram of the novel cascaded control architecture. The first step in the proposed method is related to the calculation of the virtual commands in the kinematic level using a guidance law and a FTBSC technique to ensure that the path-following error dynamics is finite-time stable. Then, the actual control inputs are designed in the dynamic layer using an AFTDO, finite-time control method, and BSC to track the desired angular velocities created by the kinematic layer and the reference surge velocity.

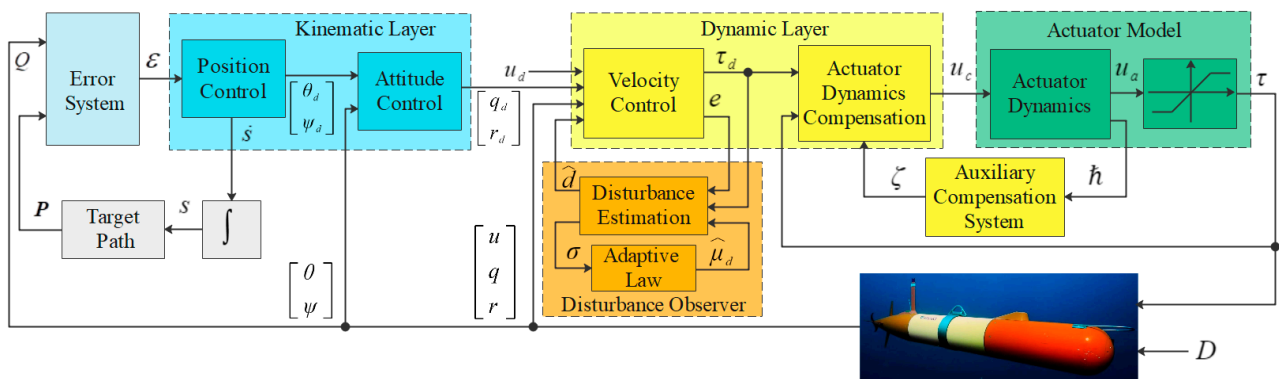


Figure 2. The block diagram of the cascaded control architecture.

3.1. Kinematic Layer

The dynamics associated with the system of path-following error expressed relative to the frame $\{F\}$ in (22) is employed now to synthesize the kinematic controller. In the kinematic layer, we compute the virtual control commands, including the movement rate of the virtual vehicle \dot{s} on the path and the desired angular rates (q_d, r_d) . The kinematic layer comprises two subsystems associated with the position control (including a guidance system) and the attitude control. The guidance system provides the desired attitude angles using FTBSC and the equivalent coordinate transformations, canceling the 3D path-following position errors (e_x, e_y, e_z) . In the attitude control subsystem, the actual pitch and yaw angles must converge to their desired values provided by the guidance system; to this end, the desired angular rates in the pitch and yaw channels will be appropriately determined via FTBSC.

3.1.1. Position Control

As the primary control objective of the 3D path-following task, defined in (23), is to cancel the off-track error $\|\epsilon\|$, we consider the following Lyapunov function:

$$V_\epsilon = \frac{1}{2} \epsilon^T \epsilon = \frac{1}{2} (e_x^2 + e_y^2 + e_z^2) \tag{24}$$

Taking the time derivate of V_ε along the trajectories of ε in (22) yields:

$$\dot{V}_\varepsilon = \varepsilon^T \dot{\varepsilon} = \varepsilon^T \left((\mathbf{S}_F)^T \varepsilon + \mathbf{R}_W^F \mathbf{V}_W - \mathbf{V}_P \right) \tag{25}$$

Since \mathbf{S}_F is a skew-symmetric matrix, one writes $\varepsilon^T (\mathbf{S}_F)^T \varepsilon = 0$. We expand (25) to obtain:

$$\begin{aligned} \dot{V}_\varepsilon &= e_x \dot{e}_x + e_y \dot{e}_y + e_z \dot{e}_z \\ &= e_x (U \cos \chi_e \cos v_e - \dot{s}) + e_y (U \sin \chi_e \cos v_e) + e_z (-U \sin v_e) \end{aligned} \tag{26}$$

Therefore, a simplified error system for the path-following position errors can be obtained using (26) as follows:

$$\begin{cases} \dot{e}_x = U \cos \chi_e \cos v_e - \dot{s} \\ \dot{e}_y = U \sin \chi_e \cos v_e \\ \dot{e}_z = -U \sin v_e \end{cases} \tag{27}$$

To cancel the off-track error, we design the evolution rate of the virtual vehicle on the path and the approach angle-based guidance laws by:

$$\begin{aligned} \dot{s} &= U \cos \chi_e \cos v_e + K_{1x} \tanh(\lambda_x e_x) + K_{2x} e_x \\ v_a &= \sin^{-1} \left(\frac{K_z \tanh(\lambda_z e_z)}{U_d} \right) \\ \chi_a &= -\sin^{-1} \left(\frac{K_y \tanh(\lambda_y e_y)}{U_d \cos v_a} \right) \end{aligned} \tag{28}$$

where $s(0) = 0$, K_{1x} , K_{2x} , λ_x , K_y , λ_y , K_z , and λ_z are positive constants satisfying $K_z \leq U_d$ and $K_y \leq U_d \cos v_{a, \max}$, with $v_{a, \max} = \sin^{-1}(K_z/U_d)$, and U_d —the desired value of the resultant velocity. Note that K_y and K_z are selected so that one obtains $\chi_a, v_a \in (-\pi/2, \pi/2)$. We can shape the dynamic responses in sway and heave by choosing appropriate values for the guidance laws' parameters. Substituting (28) into (27) yields the imposed dynamics of the path-following position errors as follows:

$$\begin{cases} \dot{e}_x = -K_{1x} \tanh(\lambda_x e_x) - K_{2x} e_x \\ \dot{e}_y = -K_y \tanh(\lambda_y e_y) + \bar{e}_\psi \\ \dot{e}_z = -K_z \tanh(\lambda_z e_z) + \bar{e}_\theta \end{cases} \tag{29}$$

with

$$\begin{aligned} \bar{e}_\psi &= -U_d \sin \chi_a (\cos v_a (1 - \cos \tilde{v}_e) + \sin v_a \sin \tilde{v}_e) \\ &\quad + \cos v_e (-U \sin \chi_a (1 - \cos \tilde{\chi}_e) + U \cos \chi_a \sin \tilde{\chi}_e + \tilde{U} \sin \chi_a) \\ \bar{e}_\theta &= -\tilde{U} \sin v_a + U (\sin v_a (1 - \cos \tilde{v}_e) - \cos v_a \sin \tilde{v}_e) \end{aligned} \tag{30}$$

where $\tilde{U} = U - U_d$, $\tilde{v}_e = v_e - v_a$, and $\tilde{\chi}_e = \chi_e - \chi_a$.

Remark 1. Works [1,4] treat the 3D path-following control problem by defining approximate course-angle errors as $\chi_e = \chi - \chi_P \approx \psi + \beta - \chi_P$ and $v_e = v - v_P \approx \theta + \alpha - v_P$, where the attack angle and the sideslip angle are given by $\alpha = -\text{atan}(w/u) \forall u > 0$ and $\beta = \text{atan}(v/\sqrt{u^2 + w^2})$, respectively. Consider the AUV's course-angle definitions as

$$\chi = \text{atan2}(\dot{y}, \dot{x}), \quad v = \text{atan} \left(-\dot{z} / \sqrt{\dot{x}^2 + \dot{y}^2} \right) \tag{31}$$

By using (11) and (31), we can conclude that $\chi = f_\chi(\theta, \psi)$ and $v = f_v(\theta)$. As a consequence, the desired attitude angles based on the approximate course-angle errors, i.e., $\psi_d = \chi_a - \beta + \chi_P$ and $\theta_d = v_a - \alpha + v_P$ are not accurate [2].

To obtain the accurate desired attitude angles (θ_d, ψ_d) , the approach angles in (28) together with two equivalent coordinate transformations are used.

The expression of the resultant velocity V_W in $\{W\}$ can be transformed into $\{F\}$ via the rotation matrix R_W^F or the rotation matrices R_E^F and R_W^E as follows:

$$R_W^F(v_a, \chi_a) V_W = R_E^F(v_P, \chi_P) R_W^E(v_d, \chi_d) V_W \quad (32)$$

with

$$R_W^E = \begin{bmatrix} \cos \chi_d \cos v_d & -\sin \chi_d & \cos \chi_d \sin v_d \\ \sin \chi_d \cos v_d & \cos \chi_d & \sin \chi_d \sin v_d \\ -\sin v_d & 0 & \cos v_d \end{bmatrix} \quad (33)$$

The AUV's desired elevation angle and azimuth angle are obtained by expanding (32):

$$\begin{cases} v_d = \text{asin}(\sin v_P \cos v_a \cos \chi_a + \cos v_P \sin v_a) \\ \chi_d = \text{atan2}(\chi_{dy}, \chi_{dx}) \end{cases} \quad (34)$$

with

$$\begin{cases} \chi_{dy} = \sin \chi_P \cos \chi_a \cos v_P \cos v_a + \cos \chi_P \sin \chi_a \cos v_a - \sin v_P \sin v_a \sin \chi_P \\ \chi_{dx} = \cos \chi_P \cos \chi_a \cos v_P \cos v_a - \sin \chi_P \sin \chi_a \cos v_a - \sin v_P \sin v_a \cos \chi_P \end{cases}$$

The expression of resultant velocity V_W in $\{W\}$ can be transformed into $\{E\}$ via the rotation matrix R_W^E or the rotation matrices R_B^E and R_W^B as follows:

$$R_W^E(v_d, \chi_d) V_W = R_B^E(\theta_d, \psi_d) R_W^B(\alpha, \beta) V_W \quad (35)$$

with

$$R_W^B = \begin{bmatrix} \cos \beta \cos \alpha & -\sin \beta \cos \alpha & -\sin \alpha \\ \sin \beta & \cos \beta & 0 \\ \cos \beta \sin \alpha & -\sin \beta \sin \alpha & \cos \alpha \end{bmatrix} \quad (36)$$

By expanding (35), one obtains the AUV's desired attitude angles:

$$\begin{cases} \theta_d = \text{asin}(\sin v_d / \cos \beta) + \alpha \\ \psi_d = \text{atan2}(\psi_{dy}, \psi_{dx}) \end{cases} \quad (37)$$

with

$$\begin{cases} \psi_{dy} = \cos \beta \cos(\theta_d - \alpha) \sin \chi_d \cos v_d - \sin \beta \cos \chi_d \cos v_d \\ \psi_{dx} = \cos \beta \cos(\theta_d - \alpha) \cos \chi_d \cos v_d + \sin \beta \sin \chi_d \cos v_d \end{cases}$$

3.1.2. Attitude Control

The angular tracking errors in the pitch and yaw channels are defined by

$$e_\theta = \theta - \theta_d, e_\psi = \psi - \psi_d \quad (38)$$

In this section, we design the AUV's desired pitch and yaw angular rates (q_d, r_d) via FTBSC to stabilize the angular tracking errors (e_θ, e_ψ) . Taking the time derivative of (38) along the trajectories of θ and ψ (expressed in (11)) yields:

$$\dot{e}_\theta = q - \dot{\theta}_d, \dot{e}_\psi = \frac{r}{\cos \theta} - \dot{\psi}_d \quad (39)$$

The virtual controls (q_d, r_d) for the kinematic layer are given by:

$$\begin{cases} q_d = -K_{1\theta}\tanh(\lambda_\theta e_\theta) - K_{2\theta}e_\theta + \dot{\theta}_d \\ r_d = \cos\theta\left(-K_{1\psi}\tanh(\lambda_\psi e_\psi) - K_{2\psi}e_\psi + \dot{\psi}_d\right) \end{cases} \quad (40)$$

where $K_{1\theta}$, $K_{2\theta}$, $K_{1\psi}$, $K_{2\psi}$, λ_θ , and λ_ψ are positive constants.

Substituting (40) into (39) yields the imposed dynamics of the attitude tracking errors:

$$\begin{cases} \dot{e}_\theta = -K_{1\theta}\tanh(\lambda_\theta e_\theta) - K_{2\theta}e_\theta + e_q \\ \dot{e}_\psi = -K_{1\psi}\tanh(\lambda_\psi e_\psi) - K_{2\psi}e_\psi + \frac{e_r}{\cos\theta} \end{cases} \quad (41)$$

where $e_q = q - q_d$ and $e_r = r - r_d$.

3.2. Dynamic Layer

The feedback control laws for the velocity of the virtual vehicle in (28) and the desired pitch and yaw rates in (40) have only been applied to the kinematics. Here, the vehicle's dynamics will be considered to extend these virtual commands. A DO-based BSC integrated with a finite-time control method is applied to calculate the actual control inputs so that the velocity tracking errors converge to a residual set around the origin within a finite time.

3.2.1. Velocity Control

We define the velocity tracking errors as follows:

$$e_v = v - v_d, v = u, q, r \quad (42)$$

where the desired surge velocity is calculated by $u_d = \sqrt{U_d^2 - (v^2 + w^2)}$.

Remark 2. A desired surge velocity is often given in the classic path-following tasks for underactuated AUVs [1,4,6,7], which fails in determining the desired resultant velocity because of drift effects in the sway and heave directions. This paper tackles this restriction so that the AUV's resultant velocity can be guaranteed to attain its given profile.

By taking the time derivative of the errors in (42) along the trajectories of u , q , and r in (12), we obtain:

$$\dot{e}_v = a_v + b_v(\tau_v - D_v(t)) - \dot{v}_d, v = u, q, r \quad (43)$$

where a_v and b_v are defined as follows:

$$\begin{cases} a_u = (m_{22}vr - m_{33}wq - f_{11}u)/m_{11}, b_u = 1/m_{11} \\ a_q = ((m_{33} - m_{11})uw - f_{55}q - Gh \sin\theta)/m_{55}, b_q = 1/m_{55} \\ a_r = ((m_{11} - m_{22})uv - f_{66}r)/m_{66}, b_r = 1/m_{66} \end{cases} \quad (44)$$

Equation (43) is rewritten with respect to the known and unknown parts as follows:

$$\dot{e}_v = \bar{a}_v + \bar{b}_v\tau_{d,v} + d_v, v = u, q, r \quad (45)$$

where $\bar{a}_v = a_v - \Delta a_v$ and $\bar{b}_v = b_v - \Delta b_v$ represent the nominal values, and Δa_v and Δb_v denote uncertainty terms in the dynamic equations; $\tau_{d,v} = \tau_v - \tilde{\tau}_v$ are the desired values of control force/moments τ_v , while the force/moments tracking errors are denoted by $\tilde{\tau}_v$; d_v are the unknown bounded lumped uncertainties consisting of the external disturbances, the force/moments tracking errors, the parameter uncertainties, and the acceleration commands:

$$d_v = \Delta a_v + \Delta b_v\tau_{d,v} + b_v(\tilde{\tau}_v - D_v) - \dot{v}_d, v = u, q, r \quad (46)$$

The virtual control law for the velocity control loop is calculated by:

$$\tau_{d,v} = -\frac{1}{\bar{b}_v} \left(\bar{a}_v + \hat{d}_v + K_{1v} \tanh(\lambda_v e_v) + K_{2v} e_v \right), v = u, q, r \quad (47)$$

where K_{1v} , K_{2v} , and λ_v are positive constants, and \hat{d}_v denote the estimations of the lumped uncertainty terms obtained by the AFTDO. The procedure for estimating the lumped uncertainties is described in the following subsection.

Let $\tilde{d}_v = d_v - \hat{d}_v$ be the lumped uncertainty estimation errors. Thus, the imposed dynamics of the velocity tracking errors is obtained by replacing (47) into (45):

$$\dot{e}_v = -K_{1v} \tanh(\lambda_v e_v) - K_{2v} e_v + \tilde{d}_v, v = u, q, r \quad (48)$$

3.2.2. Compensation of Actuator Dynamics

Let us define the force/moments tracking errors as $\tilde{\tau}_v = \tau_v - \tau_{d,v}$. By employing (13) and always working in the linear region (i.e., without the magnitude and rate saturations), their time derivatives are computed to obtain:

$$\dot{\tilde{\tau}}_v = \frac{1}{T_v} (u_{c,v} - u_{a,v}) - \dot{\tau}_{d,v}, v = u, q, r \quad (49)$$

The actual control inputs for the AUV path-following are given by:

$$u_{c,v} = u_{a,v} + T_v (\dot{\tilde{\tau}}_v - K_{a,v} \tilde{\tau}_v + \zeta_v), v = u, q, r \quad (50)$$

where $K_{a,v}$ are positive control parameters, and ζ_v denote the states of the auxiliary compensation systems (52). Substituting (50) into (49) yields

$$\dot{\tilde{\tau}}_v = -K_{a,v} \tilde{\tau}_v + \zeta_v, v = u, q, r \quad (51)$$

Control inputs exceeding the limits of the actuators cause the saturation problem. To deal with the input rate saturation, an auxiliary compensation system is introduced as follows:

$$\dot{\zeta}_v = -K_{\zeta,v} \zeta_v + \kappa_v \tilde{h}_v, v = u, q, r \quad (52)$$

where $K_{\zeta,v}$ and κ_v are positive design parameters, and $\tilde{h}_v = \dot{u}_{a,v} - (u_{c,v} - u_{a,v})/T_v$ with $\dot{u}_{a,v}$ being presented by (13).

3.3. Adaptive Fixed-Time Disturbance Observer

A continuous adaptive DO utilizing a fixed-time integral sliding surface is developed. Consider the velocity tracking error dynamics in (45) as follows:

$$\dot{e}_v = \bar{a}_v + \bar{b}_v \tau_{d,v} + d_v, v = u, q, r \quad (53)$$

Assumption 3. The lumped uncertainties d_v are bounded, i.e., there exist unknown positive constants $\mu_{d,v}$ such that $|\dot{d}_v(t)| < \mu_{d,v}, \forall t \geq 0$.

An auxiliary dynamic system is defined for the system (53) as follows:

$$\dot{\gamma}_v = \bar{a}_v + \bar{b}_v \tau_{d,v} + \hat{d}_v, v = u, q, r \quad (54)$$

We define the following integral sliding surfaces:

$$\begin{cases} \sigma_v = \tilde{d}_v + I_v \\ \dot{I}_v = l_{1v} \text{sig}^{2m-1}(\tilde{d}_v) + l_{2v} \text{sig}^{2n-1}(\tilde{d}_v), I_v(0) = 0 \end{cases}, v = u, q, r \quad (55)$$

where $\tilde{d}_v = d_v - \hat{d}_v = \dot{e}_v - \dot{\gamma}_v$, and l_{1v} , l_{2v} , m , and n are positive design parameters satisfying $0.5 < m < 1$ and $n > 1$. Taking the time derivative of (55) yields $\dot{\sigma}_v = \dot{d}_v - \dot{\hat{d}}_v + \dot{I}_v$. Therefore, the update law for the estimation of the lumped uncertainty can be given by:

$$\dot{\hat{d}}_v = \dot{I}_v + k_{1v} \text{sig}^{2m-1}(\sigma_v) + k_{2v} \text{sig}^{2n-1}(\sigma_v) + \hat{\mu}_{d,v} \tanh(\lambda_{\sigma,v} \sigma_v), \quad v = u, q, r \quad (56)$$

where k_{1v} and k_{2v} are positive constants, and the tangent hyperbolic function is used instead of the discontinuous signum function to eliminate the chattering; $\hat{\mu}_{d,v}$ denotes the estimation of $\mu_{d,v}$ which is adaptively updated by

$$\dot{\hat{\mu}}_{d,v} = -\xi_{1v} \hat{\mu}_{d,v} - \xi_{2v} \hat{\mu}_{d,v}^{2n-1} + \xi_{0v} |\sigma_v|, \quad \hat{\mu}_{d,v}(0) \geq 0 \quad (57)$$

Thus, the imposed dynamics of sliding surface σ_v is expressed as follows:

$$\dot{\sigma}_v = -k_{1v} \text{sig}^{2m-1}(\sigma_v) - k_{2v} \text{sig}^{2n-1}(\sigma_v) - \hat{\mu}_{d,v} \tanh(\lambda_{\sigma,v} \sigma_v) + \dot{d}_v \quad (58)$$

Theorem 1. *If we employ the AFTDO in (56) with the adaptive law (57) to estimate the lumped uncertainties in the system (53) under Assumption 3, the disturbance estimation error \tilde{d}_v uniformly converges to an arbitrarily small region around zero, i.e., $\Omega_{d,v}$ in (70), within a fixed time no greater than $t_{r,v} + t_{s,v}$, where $t_{r,v}$ in (64) is the time needed for the sliding variable σ_v to reach the bounded region $\Omega_{\sigma,v}$ in (65), and $t_{s,v}$ in (69) denotes the settling time of the disturbance estimation error \tilde{d}_v .*

Proof. Consider the Lyapunov function $V_{\sigma,v} = \frac{1}{2} \sigma_v^2 + \frac{1}{2\xi_{0v}} \tilde{\mu}_{d,v}^2$, $v = u, q, r$, where $\tilde{\mu}_{d,v} = \mu_{d,v} - \hat{\mu}_{d,v}$ denotes the (adaptive parameter) estimation error. By taking the time derivative of $V_{\sigma,v}$ and substituting (57) and (58) into it, we obtain:

$$\begin{aligned} \dot{V}_{\sigma,v} &= \sigma_v \dot{\sigma}_v + \frac{1}{\xi_{0v}} \tilde{\mu}_{d,v} \dot{\tilde{\mu}}_{d,v} = \sigma_v \dot{\sigma}_v - \frac{1}{\xi_{0v}} \tilde{\mu}_{d,v} \dot{\hat{\mu}}_{d,v} \\ &= \sigma_v \left(-k_{1v} \text{sig}^{2m-1}(\sigma_v) - k_{2v} \text{sig}^{2n-1}(\sigma_v) - \hat{\mu}_{d,v} \tanh(\lambda_{\sigma,v} \sigma_v) + \dot{d}_v \right) \\ &\quad - \frac{1}{\xi_{0v}} \tilde{\mu}_{d,v} \left(-\xi_{1v} \hat{\mu}_{d,v} - \xi_{2v} \hat{\mu}_{d,v}^{2n-1} + \xi_{0v} |\sigma_v| \right) \\ &\leq -k_{1v} \sigma_v^{2m} - k_{2v} \sigma_v^{2n} + \frac{\xi_{1v}}{\xi_{0v}} \tilde{\mu}_{d,v} \hat{\mu}_{d,v} + \frac{\xi_{2v}}{\xi_{0v}} \tilde{\mu}_{d,v} \hat{\mu}_{d,v}^{2n-1} + \frac{\tilde{\mu}_{d,v} \dot{d}_v}{\lambda_{\sigma,v}} \end{aligned} \quad (59)$$

In the process of obtaining an upper bound for the term $\tilde{\mu}_{d,v} \hat{\mu}_{d,v}^{2n-1}$ by Lemma 5, a key condition must be met, i.e., $\hat{\mu}_{d,v} = \mu_{d,v} - \tilde{\mu}_{d,v} \geq 0$. This condition can be checked by applying Lemma 4 to the adaptive law (57). Then, employing Lemma 5 yields

$$\tilde{\mu}_{d,v} \hat{\mu}_{d,v}^{2n-1} = \tilde{\mu}_{d,v} (\mu_{d,v} - \tilde{\mu}_{d,v})^{2n-1} \leq \frac{2n-1}{2n} \left(\mu_{d,v}^{2n} - \tilde{\mu}_{d,v}^{2n} \right) \quad (60)$$

According to the definition of $\hat{\mu}_{d,v}$ and by using Young's inequality, we have

$$\tilde{\mu}_{d,v} \hat{\mu}_{d,v} = \tilde{\mu}_{d,v} (\mu_{d,v} - \tilde{\mu}_{d,v}) \leq \frac{1}{2} \mu_{d,v}^2 - \frac{1}{2} \tilde{\mu}_{d,v}^2 \quad (61)$$

To ensure the fixed-time stability of the proposed observer, only the term $-\frac{1}{2} \tilde{\mu}_{d,v}^2$ remains to be transformed into the appropriate form. Consider Lemma 6 and let $x = \frac{1}{2\xi_{0v}} \tilde{\mu}_{d,v}^2$, $y = 1$, $a = m$, $b = 1 - m$, and $c = 1/m$. Therefore, the following inequality is obtained:

$$\left(\frac{\tilde{\mu}_{d,v}^2}{2\xi_{0v}} \right)^m \leq \frac{\tilde{\mu}_{d,v}^2}{2\xi_{0v}} + (1 - m) m^{\frac{m}{1-m}} \quad (62)$$

We rewrite (59) using (60)–(62) and (9)–(10) in Lemma 7 as follows:

$$\begin{aligned} \dot{V}_{\sigma,\nu} &\leq -2^m k_{1\nu} \left(\frac{\sigma_\nu^2}{2}\right)^m - 2^n k_{2\nu} \left(\frac{\sigma_\nu^2}{2}\right)^n - \xi_{1\nu} \left(\frac{\hat{\mu}_{d,\nu}^2}{2\xi_{0\nu}}\right)^m - \frac{(2n-1)(2\xi_{0\nu})^{n-1}\xi_{2\nu}}{n} \left(\frac{\hat{\mu}_{d,\nu}^2}{2\xi_{0\nu}}\right)^n \\ &\quad + \xi_{1\nu} \left(\frac{\mu_{d,\nu}^2}{2\xi_{0\nu}} + (1-m)m^{\frac{m}{1-m}}\right) + \frac{(2n-1)\xi_{2\nu}}{2n\xi_{0\nu}} \mu_{d,\nu}^{2n} + \frac{\hat{\mu}_{d,\nu}^l}{\lambda_{\sigma,\nu}} \\ &\leq -\Lambda_{1\nu} V_{\sigma,\nu}^m - \Lambda_{2\nu} V_{\sigma,\nu}^n + \Delta_{\sigma,\nu} \end{aligned} \tag{63}$$

where

$$\begin{aligned} \Lambda_{1\nu} &= \min\{2^m k_{1\nu}, \xi_{1\nu}\}, \quad \Lambda_{2\nu} = \min\left\{2k_{2\nu}, \frac{(2n-1)\xi_{0\nu}^{n-1}\xi_{2\nu}}{n}\right\} \\ \Delta_{\sigma,\nu} &= \xi_{1\nu} \left(\frac{\mu_{d,\nu}^2}{2\xi_{0\nu}} + (1-m)m^{\frac{m}{1-m}}\right) + \frac{(2n-1)\xi_{2\nu}}{2n\xi_{0\nu}} \mu_{d,\nu}^{2n} + \frac{\hat{\mu}_{d,\nu}^l}{\lambda_{\sigma,\nu}} \end{aligned}$$

According to Lemma 3, the practically fixed-time stability conditions for the sliding variable σ_ν is met, i.e., the trajectory of the sliding variable converges within a fixed time into an arbitrarily bounded region around the origin characterized by

$$t_{r,\nu} \leq \frac{1}{\Lambda_{1\nu}\eta_{\sigma,\nu}(1-m)} + \frac{1}{\Lambda_{2\nu}\eta_{\sigma,\nu}(n-1)} \tag{64}$$

$$\Omega_{\sigma,\nu} = \left\{ (\sigma_\nu, \mu_{d,\nu}) \mid V_{\sigma,\nu} \leq \min\left\{ \left(\frac{\Delta_{\sigma,\nu}}{\Lambda_{1\nu}(1-\eta_{\sigma,\nu})}\right)^{\frac{1}{m}}, \left(\frac{\Delta_{\sigma,\nu}}{\Lambda_{2\nu}(1-\eta_{\sigma,\nu})}\right)^{\frac{1}{n}} \right\} \right\} \tag{65}$$

where $0 < \eta_{\sigma,\nu} < 1$. Also, it follows that the rate of the sliding variable is bounded in $\Omega_{\sigma,\nu}$, i.e., there exists a positive constant $\mu_{\sigma,\nu}$ such that $|\dot{\sigma}_\nu(t)| \leq \mu_{\sigma,\nu}, \forall t \geq t_{r,\nu}$.

We take the time derivative of the sliding variable in (55) to obtain the dynamics of disturbance estimation errors:

$$\dot{\tilde{d}}_\nu = -l_{1\nu} \text{sig}^{2m-1}(\tilde{d}_\nu) - l_{2\nu} \text{sig}^{2n-1}(\tilde{d}_\nu) + \dot{\sigma}_\nu \tag{66}$$

Define the Lyapunov function as $V_{d,\nu} = 0.5\tilde{d}_\nu^2, \nu = u, q, r$. By taking the time derivative of $V_{d,\nu}$ and substituting from (66), one has

$$\dot{V}_{d,\nu} \leq -l_{1\nu}\tilde{d}_\nu^{2m} - l_{2\nu}\tilde{d}_\nu^{2n} + |\tilde{d}_\nu|\mu_{\sigma,\nu} \tag{67}$$

We rewrite (67) using Lemma 6 (with $x = \tilde{d}_\nu, y = \mu_{\sigma,\nu}, a = b = 1$, and $c = 0.1$) and then (8) in Lemma 7 to obtain:

$$\dot{V}_{d,\nu} \leq -\Phi_{1\nu} V_{d,\nu}^m - \Phi_{2\nu} V_{d,\nu}^n + \Delta_{d,\nu} \tag{68}$$

where $\Phi_{1\nu} = 2^m(l_{1\nu} - 0.05), \Phi_{2\nu} = 2^n(l_{2\nu} - 0.05)$, and $\Delta_{d,\nu} = 5\mu_{\sigma,\nu}^2$. The parameters $l_{1\nu}$ and $l_{2\nu}$ are selected such that $\Phi_{1\nu} > 0$ and $\Phi_{2\nu} > 0$.

By applying Lemma 3, we can conclude that the trajectory of disturbance estimation error converges within a fixed time into an arbitrarily bounded region around the origin described by

$$t_{s,\nu} \leq \frac{1}{\Phi_{1\nu}\eta_{d,\nu}(1-m)} + \frac{1}{\Phi_{2\nu}\eta_{d,\nu}(n-1)} \tag{69}$$

$$\Omega_{d,\nu} = \left\{ \tilde{d}_\nu \mid V_{d,\nu} \leq \min\left\{ \left(\frac{\Delta_{d,\nu}}{\Phi_{1\nu}(1-\eta_{d,\nu})}\right)^{\frac{1}{m}}, \left(\frac{\Delta_{d,\nu}}{\Phi_{2\nu}(1-\eta_{d,\nu})}\right)^{\frac{1}{n}} \right\} \right\} \tag{70}$$

where $0 < \eta_{d,\nu} < 1$. \square

4. Stability Analysis

The following theorem summarizes the stability conditions for the path-following of underactuated AUVs in the presence of lumped uncertainties and actuator limits.

Theorem 2. Consider the underactuated AUV model in (11)–(13) under Assumptions 1 and 2. Suppose the kinematic controller laws are designed as (28) and (40), and the dynamic controller laws are described as (47) and (50) with the auxiliary compensation system (52). In this case, the cascaded closed-loop system is uniformly stable and the path-following errors converge to an arbitrarily small region around zero within a finite time.

Proof. To begin with, we divide the cascaded closed-loop system into three subsystems: (1) the first subsystem, which contains the position control loops, attitude control loops, and velocity control loops; (2) the second subsystem, including the actuator dynamics compensation loops and auxiliary compensation systems; (3) the third subsystem, consisting of the disturbance observers. Here, the stability analysis relies on the premise that the AFTDO can provide a quick and accurate estimation of the lumped uncertainty in a fixed time.

Remark 3. By referring to (71), it is clear that the dynamics of the actuator dynamics compensation loops and auxiliary compensation systems do not contain the nonlinear terms, and hence, do not meet the finite-time stability conditions. Note that according to (46), the errors of the actuator dynamics compensation loops, i.e., $\tilde{\tau}_v$, $v = u, q, r$, appear in the lumped uncertainties. Hence, their effects on the velocity tracking error dynamics can be compensated by the AFTDO in a fixed time. Therefore, to ensure the finite-time stability of the path-following errors, we do not need to prove that the second subsystem is finite-time stable, but only that the errors $\tilde{\tau}_v$ are uniformly bounded.

First, we consider the systems (51) and (52) as the second subsystem:

$$\begin{cases} \dot{\tilde{\tau}}_v = -K_{a,v}\tilde{\tau}_v + \zeta_v \\ \dot{\zeta}_v = -K_{\zeta,v}\zeta_v + \kappa_v\tilde{h}_v \end{cases}, v = u, q, r \quad (71)$$

Define a second Lyapunov function as $V_2 = 0.5(\tilde{\tau}_u^2 + \tilde{\tau}_q^2 + \tilde{\tau}_r^2 + \zeta_u^2 + \zeta_q^2 + \zeta_r^2)$. Taking its time derivative, substituting from (71), and using Young's inequality, one has

$$\begin{aligned} \dot{V}_2 &\leq -\left(K_{a,u} - \frac{1}{2}\right)\tilde{\tau}_u^2 - \left(K_{a,q} - \frac{1}{2}\right)\tilde{\tau}_q^2 - \left(K_{a,r} - \frac{1}{2}\right)\tilde{\tau}_r^2 - \left(K_{\zeta,u} - \frac{1+\kappa_u}{2}\right)\zeta_u^2 \\ &\quad - \left(K_{\zeta,q} - \frac{1+\kappa_q}{2}\right)\zeta_q^2 - \left(K_{\zeta,r} - \frac{1+\kappa_r}{2}\right)\zeta_r^2 + \frac{\kappa_u}{2}\tilde{h}_u^2 + \frac{\kappa_q}{2}\tilde{h}_q^2 + \frac{\kappa_r}{2}\tilde{h}_r^2 \\ &\leq -\Gamma_1 V_2 + \Gamma_0 \end{aligned} \quad (72)$$

where

$$\begin{aligned} \Gamma_1 &= 2\min\left\{\left(K_{a,u} - \frac{1}{2}\right), \left(K_{a,q} - \frac{1}{2}\right), \left(K_{a,r} - \frac{1}{2}\right), \left(K_{\zeta,u} - \frac{1+\kappa_u}{2}\right), \left(K_{\zeta,q} - \frac{1+\kappa_q}{2}\right), \left(K_{\zeta,r} - \frac{1+\kappa_r}{2}\right)\right\} \\ \Gamma_0 &= \frac{\kappa_u}{2}\tilde{h}_u^2 + \frac{\kappa_q}{2}\tilde{h}_q^2 + \frac{\kappa_r}{2}\tilde{h}_r^2 \end{aligned}$$

The control gains can be selected so that $\Gamma_1 > 0$. By assuming that \tilde{h}_v , $v = u, q, r$, are bounded, it follows that the system (71) is uniformly bounded.

Now, consider the following candidate Lyapunov function for the first subsystem:

$$V_1 = \frac{1}{2}\left(e_x^2 + e_y^2 + e_z^2 + e_\theta^2 + e_\psi^2 + e_u^2 + e_q^2 + e_r^2\right) \quad (73)$$

By taking the time derivative of V_1 , substituting from (29), (41), and (48), and applying Lemma 1, we have:

$$\begin{aligned} \dot{V}_1 \leq & -K_{1x}|e_x| - K_{2x}e_x^2 + \frac{K_{x^t}}{\lambda_x} - K_y|e_y| + \frac{K_{y^t}}{\lambda_y} + |e_y||\bar{e}_\psi| - K_z|e_z| + \frac{K_{z^t}}{\lambda_z} + |e_z||\bar{e}_\theta| - K_{1\theta}|e_\theta| \\ & - K_{2\theta}e_\theta^2 + \frac{K_{1\theta^t}}{\lambda_\theta} + |e_\theta||e_q| - K_{1\psi}|e_\psi| - K_{2\psi}e_\psi^2 + \frac{K_{1\psi^t}}{\lambda_\psi} + \frac{|e_\psi||e_r|}{\cos\theta_{\max}} - K_{1u}|e_u| - K_{2u}e_u^2 + \frac{K_{1u^t}}{\lambda_u} \\ & + |e_u||\bar{d}_u| - K_{1q}|e_q| - K_{2q}e_q^2 + \frac{K_{1q^t}}{\lambda_q} + |e_q||\bar{d}_q| - K_{1r}|e_r| - K_{2r}e_r^2 + \frac{K_{1r^t}}{\lambda_r} + |e_r||\bar{d}_r| \end{aligned} \quad (74)$$

According to Theorem 1, the disturbance estimation errors converge within a fixed time no greater than $t_0 = \max_v\{t_{r,v} + t_{s,v}\}$ to an arbitrarily bounded region around the origin, i.e., $|\bar{d}_v| < \bar{\delta}_v, \forall t \geq t_0$. Also, we can assume that $|\bar{e}_\psi| \leq \delta_\psi$ and $|\bar{e}_\theta| \leq \delta_\theta, \forall t \geq 0$, and $|e_q| \leq \delta_q, |e_r|/\cos\theta_{\max} \leq \delta_r, |\bar{d}_u| \leq \bar{\delta}_u, |\bar{d}_q| \leq \bar{\delta}_q, \text{ and } |\bar{d}_r| \leq \bar{\delta}_r, \forall t \geq t_0$. Therefore, we rewrite (74) using (9) in Lemma 7 in the following form:

$$\begin{aligned} \dot{V}_1 \leq & -K_{1x}|e_x| - (K_y - \delta_\psi)|e_y| - (K_z - \delta_\theta)|e_z| - (K_{1\theta} - \delta_q)|e_\theta| - (K_{1\psi} - \delta_r)|e_\psi| \\ & - (K_{1u} - \bar{\delta}_u)|e_u| - (K_{1q} - \bar{\delta}_q)|e_q| - (K_{1r} - \bar{\delta}_r)|e_r| + \frac{K_{1x^t}}{\lambda_x} + \frac{K_{y^t}}{\lambda_y} + \frac{K_{z^t}}{\lambda_z} + \frac{K_{1\theta^t}}{\lambda_\theta} \\ & + \frac{K_{1\psi^t}}{\lambda_\psi} + \frac{K_{1u^t}}{\lambda_u} + \frac{K_{1q^t}}{\lambda_q} + \frac{K_{1r^t}}{\lambda_r} \leq KV_1^{0.5} + \Delta \end{aligned} \quad (75)$$

where

$$\begin{aligned} K &= \sqrt{2}\min\{K_{1x}, (K_y - \delta_\psi), (K_z - \delta_\theta), (K_{1\theta} - \delta_q), (K_{1\psi} - \delta_r), (K_{1u} - \bar{\delta}_u), (K_{1q} - \bar{\delta}_q), (K_{1r} - \bar{\delta}_r)\} \\ \Delta &= \frac{K_{1x^t}}{\lambda_x} + \frac{K_{y^t}}{\lambda_y} + \frac{K_{z^t}}{\lambda_z} + \frac{K_{1\theta^t}}{\lambda_\theta} + \frac{K_{1\psi^t}}{\lambda_\psi} + \frac{K_{1u^t}}{\lambda_u} + \frac{K_{1q^t}}{\lambda_q} + \frac{K_{1r^t}}{\lambda_r} \end{aligned}$$

To ensure stability, the control parameters can be selected so that $K > 0$. According to Lemma 2, the first subsystem is practically finite-time stable, meaning that the path-following errors converge to the bounded set Ω around the origin in the finite time t_s , described as

$$\Omega = \left\{ \mathbf{x} \left| V_1^{0.5}(\mathbf{x}) \leq \frac{\Delta}{K(1-\eta)} \right. \right\}, t_s \leq \frac{V_1^{0.5}(\mathbf{x}_0)}{0.5K\eta} \quad (76)$$

where $0 < \eta < 1, \mathbf{x} = [e_x, e_y, e_z, e_\theta, e_\psi, e_u, e_q, e_r]$, and \mathbf{x}_0 is the initial conditions. \square

Remark 4. In general, the control parameters of the kinematic controller are selected so that the performance indices in terms of convergence time and robustness are met. The parameters of the dynamic controller must be chosen high enough to accurately track the desired velocities provided by the kinematic layer. In particular, increasing the tracking loops' parameters $K_{1x}, K_{2x}, \lambda_x, K_y, K_z, \lambda_y, \lambda_z, K_{1\theta}, K_{2\theta}, K_{1\psi}, K_{2\psi}, \lambda_\theta, \lambda_\psi, K_{1u}, K_{2u}, K_{2q}, K_{2r}, \lambda_v, K_{a,v}$, the observers' parameters $k_{1v}, k_{2v}, \xi_{0v}, \xi_{1v}, \xi_{2v}, l_{1v}, l_{2v}, \lambda_{\sigma,v}, n$, and reducing the parameter m will enhance the convergence rate and reduce the steady-state errors. However, issues such as actuator saturation and discontinuous control inputs should be taken into account in adjusting these parameters. Also, a trade-off between convergence time and magnitude/rate saturation management property should be made to adjust the gains of auxiliary compensation system $K_{\zeta,v}, \kappa_v$.

Remark 5. The course-angle errors χ_e and v_e must be available to calculate the velocity of the virtual vehicle on the path, i.e., \dot{s} in (28). Although these errors can be obtained by the equivalent coordinate transformations among the flow frame $\{W\}$, body-fixed frame $\{B\}$, and Earth-fixed frame $\{E\}$, we use their desired values, i.e., the approach angles χ_a and v_a , instead of them to simplify the calculations.

5. Numerical Simulations

To demonstrate the capabilities of the introduced control scheme, numerical simulations for path-following control of an underactuated AUV considering model uncertainties, external disturbances, and actuator limits are carried out based on the Mat-

lab/Simulink platform under different working conditions, given in Table 1. Table 2 lists the model parameters of the AUV [2]. The actuator magnitudes are saturated within $0 \leq \tau_u \leq 2500$ N, $|\tau_q| \leq 3500$ Nm, and $|\tau_r| \leq 3500$ Nm, and their rates are limited to ± 1500 N/s(Nm/s). The actuators' time constant is $T_v = 0.25$ s. We assume that there exist $\pm 20\%$ uncertainties in the model parameters (-20% for G , h , and $m_{(\cdot)}$, and $+20\%$ for $f_{(\cdot)}$). The AUV's desired resultant velocity is $U_d = 2$ m/s. The parameters of the tracking loops and auxiliary compensation systems are selected as $K_{1x} = K_{2x} = 0.2$, $\lambda_x = 5$, $K_y = K_z = 0.2$, $\lambda_y = \lambda_z = 1.2$, $K_{1\theta} = K_{2\theta} = K_{1\psi} = K_{2\psi} = 0.3$, $\lambda_\theta = \lambda_\psi = 1.5$, $K_{1v} = 0.07$, $K_{2u} = 0.05$, $K_{2q} = K_{2r} = 0.1$, $\lambda_\theta = \lambda_\psi = 1.5$, $K_{1v} = 0.07$, $K_{2u} = 0.05$, $K_{2q} = K_{2r} = 0.1$, $\lambda_v = 10$, $K_{a,v} = 0.6$, $K_{\zeta,v} = 0.3$, $\kappa_v = 5$, and the AFTDO gains are set as $l_{1,v} = l_{2,v} = 0.1$, $k_{1,v} = k_{2,v} = 0.1$, $\lambda_{\sigma,v} = 25$, $\zeta_{0v} = 15$, $\zeta_{1v} = \zeta_{2v} = 0.1$, $m = 0.8$, $n = 1.2$, with $v = u, q, r$.

Table 1. Working conditions for the validation of the control architecture.

Condition	Description	Range [s]
(1)	Nominal parameters, without external disturbances	$0 \leq t < 150$
(2)	Parameter uncertainties & constant external disturbances	$150 \leq t < 300$
(3)	Parameter uncertainties & varying external disturbances	$300 \leq t \leq 450$

Table 2. Model parameters of the AUV.

$G = 10,681$ N	$m_{55} = 4061$ kgm ²	$f_{22} = 138$ kg/s
$m_{11} = 1116$ kg	$m_{66} = 4061$ kgm ²	$f_{33} = 138$ kg/s
$m_{22} = 2133$ kg	$h = 0.0065$ m	$f_{55} = 490$ kgm ² /s
$m_{33} = 2133$ kg	$f_{11} = 25.5$ kg/s	$f_{66} = 490$ kgm ² /s

5.1. Scenario 1

In this scenario, comparative simulations are carried out for the path-following of a 3D straight path between the proposed controller and two BSC-based controllers (FTBSC and BSC) to evaluate the performance of the guidance system and the control robustness. FTBSC has the same tracking loops as the proposed controller and BSC is formed based on the conventional backstepping control with the same position control law as the proposed controller. FTBSC and BSC do not benefit from disturbance observers and auxiliary compensation systems. For fair comparison, the control gains are adjusted such that the maximum amplitude of control efforts under Condition (1) falls within the same range. The AUV's initial conditions are set as $x(0) = 5$ m, $y(0) = 10$ m, $z(0) = 55$ m, $\theta(0) = \psi(0) = 0$ deg, $u(0) = 0.1$ m/s, $v(0) = w(0) = 0$ m/s, $q(0) = r(0) = 0$ deg/s. The straight target path is parameterized as $x_P(s) = s$, $y_P(s) = 5$, and $z_P(s) = 50$. The external disturbances are presented by [1]

$$\begin{cases} D_u(t) = +0.2m_{11}D(t) \text{ N} \\ D_v(t) = -0.1m_{22}D(t) \text{ N} \\ D_w(t) = +0.1m_{33}D(t) \text{ N} \\ D_q(t) = -0.1m_{55}D(t) \text{ Nm} \\ D_r(t) = +0.2m_{66}D(t) \text{ Nm} \end{cases} \quad (77)$$

where $D(t) = 0.3$ for the constant disturbances and $D(t) = 0.2 + 0.1 \sin(0.2t)$ for the fast time-varying disturbances.

Figures 3–6 present the comparative simulation results of Scenario 1. Figure 3 shows the 3D path-following of the AUV. Tracking errors of positions, attitudes, and velocities are given in Figure 4. Figure 5 illustrates the control force and moments. The disturbance estimation errors and adaptive parameter estimations are depicted in Figure 6. Figures 3 and 4

show that the AUV under all controllers can reach and follow the path in conditions (1), but the presented scheme, due to its more robust dynamic controller, outperforms FTBSC and BSC in the presence of parameter uncertainties and external disturbances in Conditions (2) and (3). The proposed scheme can completely reject the constant external disturbances and confine the path-following errors to a small region around the origin with time-varying external disturbances. Moreover, FTBSC fulfills the task better than BSC, which can be attributed to the robust properties of tangent hyperbolic functions in the attitude and velocity tracking loops. Note that the along-tracking is more accurate for all controllers since, unlike the trajectory-tracking task, and according to (29), the along-tracking error e_x dynamics is unaffected by the attitude tracking errors and thus the lumped uncertainties. Also, the larger external disturbance in the yaw motion compared to the pitch motion in (77) has resulted in larger errors in e_y than in e_z . Referring to Figure 6, accurate and fast estimation of the lumped uncertainties by the AFTDO is an important factor in enhancing the robustness of the proposed controller. The control inputs in Figure 5 are constrained to acceptable unsaturated regions for all controllers, and due to the use of the hyperbolic tangent function instead of the sign function, chattering does not appear in the control inputs. Also, by comparing the control effort amplitudes of different controllers under condition (1), this insight can be gained by pointing out that the better performance of the proposed controller is not due to higher control gains but rather its specific control law. Figure 6 shows that the adaptive law in (57) can quickly track the changes in the lumped uncertainty and provide an upper bound for the rate of lumped uncertainty.

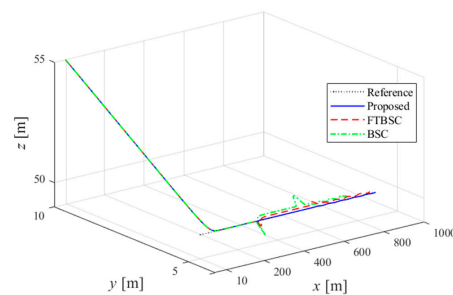


Figure 3. 3D straight path-following in Scenario 1.

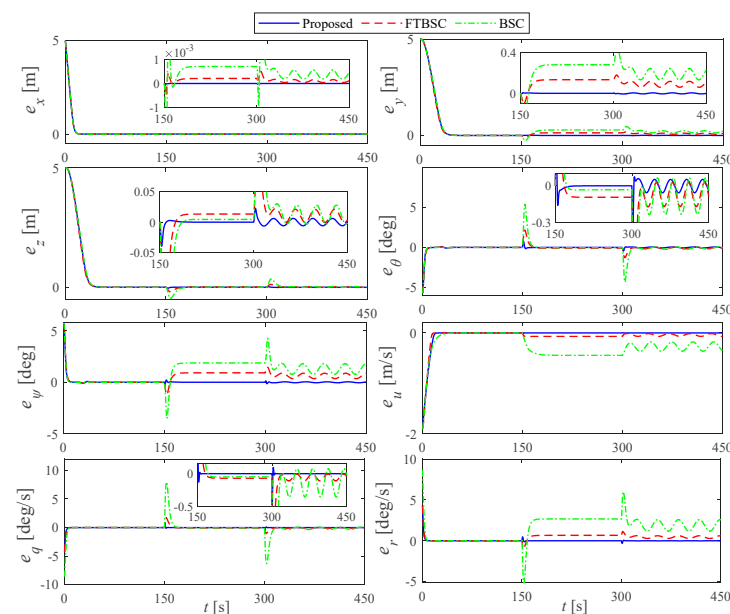


Figure 4. Position, attitude, and velocity tracking errors in Scenario 1.

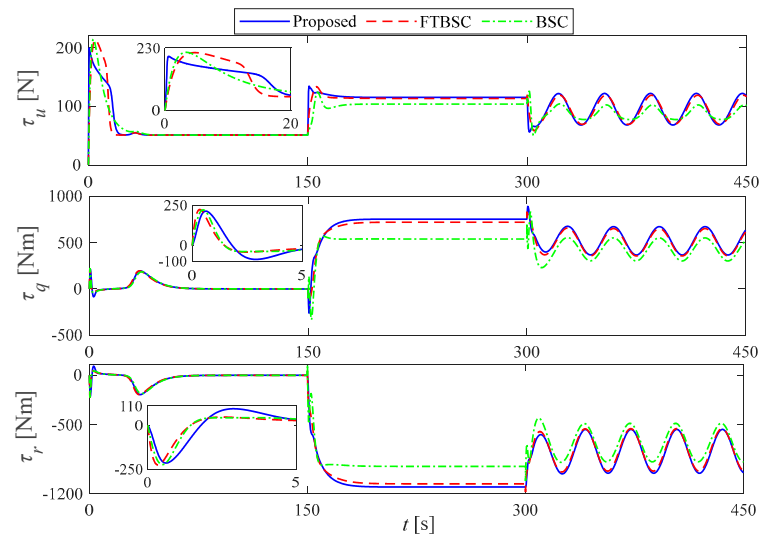


Figure 5. Control force and moments in Scenario 1.

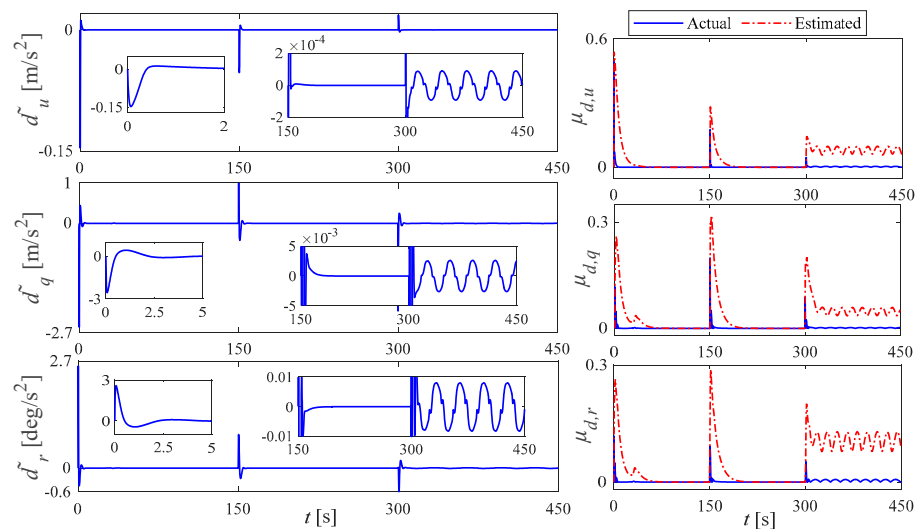


Figure 6. Disturbance estimation errors and adaptive parameter estimation for the proposed control in Scenario 1.

5.2. Scenario 2

In this scenario, comparative simulations between the proposed controller and a traditional disturbance observer-based backstepping control (DOBSC) are carried out to further study the advantages of the presented control method, considering more challenging situations in terms of the target path to be followed, the external disturbances, and the initial conditions. A circular helix target path of radius R and slope R/b is parameterized as $x_p(s) = R \cos(s/\sqrt{R^2 + b^2})$, $y_p(s) = R \sin(s/\sqrt{R^2 + b^2})$, $z_p(s) = bs/\sqrt{R^2 + b^2}$, with $R = 80$ m, $b = 5/\pi$ m. The AUV's initial states are $x(0) = 110$ m, $y(0) = 30$ m, $z(0) = -30$ m, $\theta(0) = \psi(0) = -45$ deg, $u(0) = 0.1$ m/s, $v(0) = w(0) = 0$ m/s, $q(0) = r(0) = 0$ deg/s. Equation (77) presents the external disturbances, with $D(t) = 0.5$ for the constant disturbances and $D(t) = 0.35 + 0.3 \sin(0.2t)$ for the fast time-varying disturbances.

The simulation results of Scenario 2 are presented in Figures 7–10. Figure 7 depicts the 3D path-following of the AUV. Tracking errors of positions, attitudes, and velocities are given in Figure 8. Figure 9 illustrates the control force and moments. The disturbance estimation errors are shown in Figure 10. As shown in Figure 8, it is easy to see that both schemes eliminate the effect of constant environmental disturbances and confine the

impact of time-varying external disturbances on the path-following errors to a small region around zero. Therefore, we can say that the path-following and surge velocity tracking errors converge to a region around zero in all conditions. However, the tracking accuracy and robustness of the proposed finite-time controller are better than those of the DOBSC. According to Figure 9, the oscillations in the control force and moments associated with the transient states of Condition (1) for the proposed method are lower than the corresponding values for the DOBSC. This is because the hyperbolic tangent functions confine the control inputs for large initial errors and meanwhile provide appropriate convergence rates for all times of state trajectories. The proposed control gains can be chosen with less conservatism with respect to the actuator limitations; as a consequence of this, we can use all the capacity of the system’s actuators for a larger range of initial conditions. As depicted in Figure 10, both observers can fulfill the estimation task, but the AFTDO has higher capability to deal with the lumped uncertainties in terms of convergence speed and estimation accuracy; there exist oscillations with large overshoots and low damping rates in the estimations by the DOBSC.

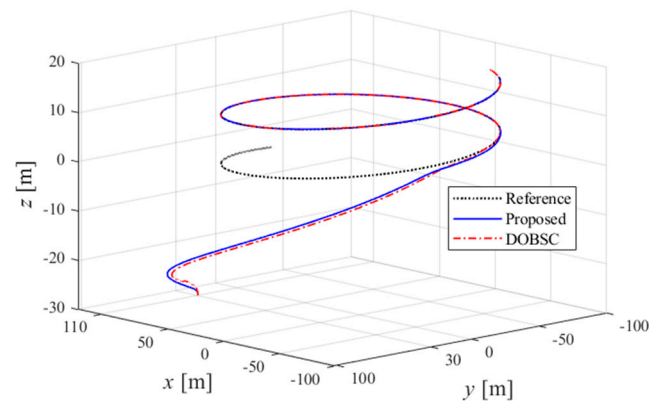


Figure 7. Helix path-following in Scenario 2.

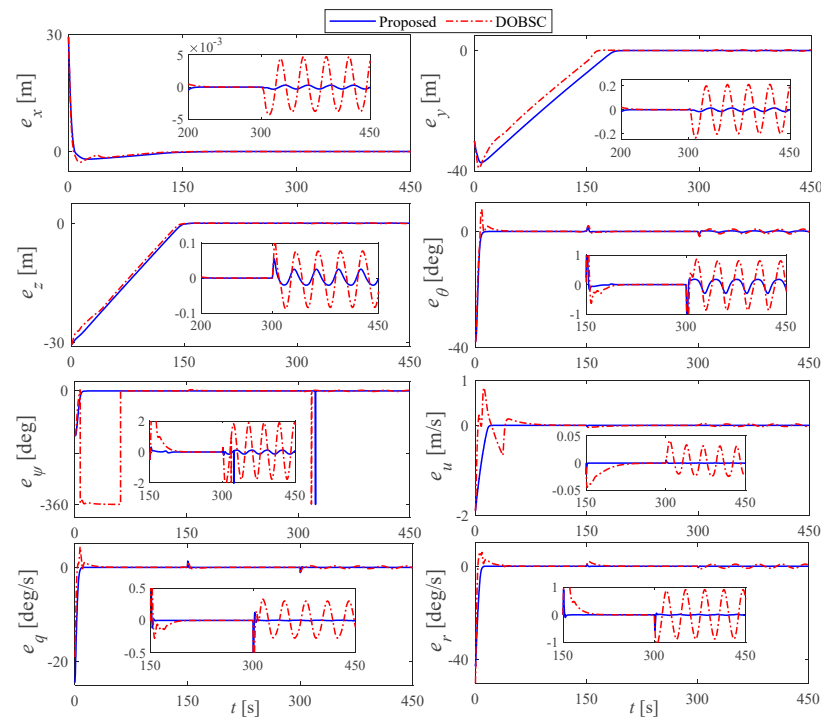


Figure 8. Position, attitude, and velocity tracking errors in Scenario 2.

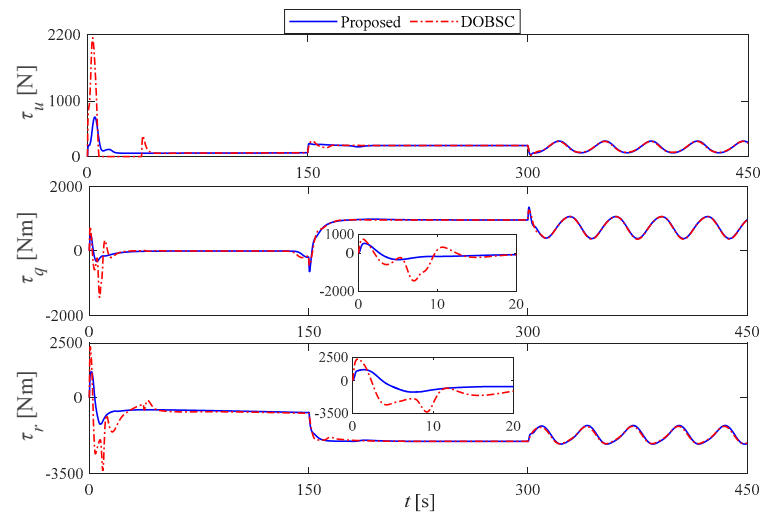


Figure 9. Control force and moments in Scenario 2.

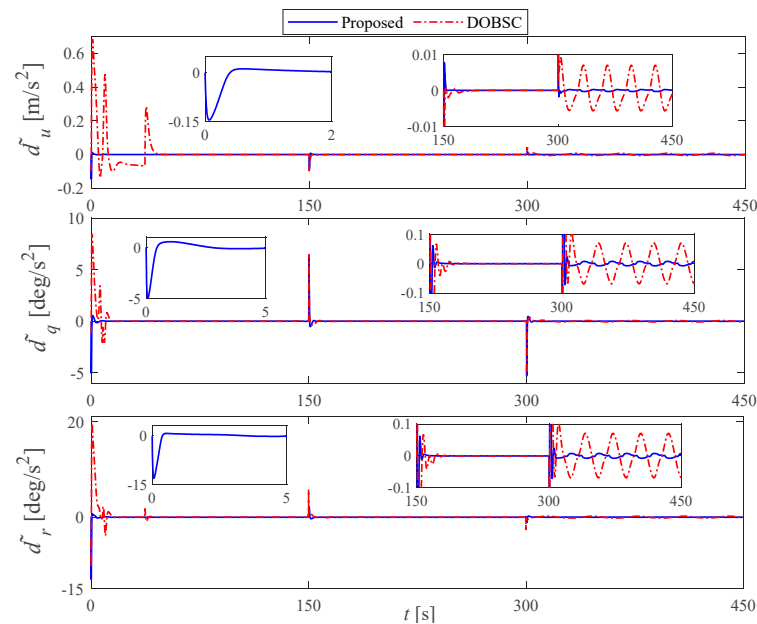


Figure 10. Disturbance estimation errors in Scenario 2.

Also, it is easy to see from Figure 10 that the disturbance estimation errors \tilde{d}_v tend to zero with constant lumped disturbances (Condition 2). We can deduce this result by referring to (58) and (66), where the dynamics of the disturbance estimation errors are driven by the lumped uncertainty rates \dot{d}_v . Thus, if the disturbances are time-invariant, i.e., $\dot{d}_v = 0$, complete compensation by AFTDO and exact convergence are achieved. However, ocean currents typically induce time-varying perturbations, the fast-varying sinusoidal functions being the common forms of the external disturbances acting on AUVs [1,8,39].

5.3. Scenario 3

A comparative simulation between two versions of the proposed controller (i.e., the controller without the auxiliary compensation system, called Proposed 1, and the controller equipped with the auxiliary compensation system in (52), called Proposed 2) is conducted to evaluate the control performance for tighter constraints on the input rates. The target path and the initial conditions are the same as those in Scenario 2. The constraints on input rates are reduced to ± 400 N/s, ± 450 Nm/s, ± 800 Nm/s for the surge control input,

pitch control input, and yaw control input, respectively. Figure 11 presents the control input magnitudes/rates for the tighter constraints on input rates, where the input rates are calculated by $(u_{c,v} - u_{a,v})/T_v$, i.e., the rates of actuator states in (13) before the saturation block. This figure shows that the maximum values of the input rates for Proposed 1 far exceed the saturation limits. Due to the auxiliary compensation system, Proposed 2 can reduce the maximum values of the input rates considerably and take the inputs out of the saturation zone sooner. Therefore, the proposed auxiliary compensation system can effectively manipulate the control signals when exceeding hard constraints on input rates, resulting in higher robustness and smoother control inputs.

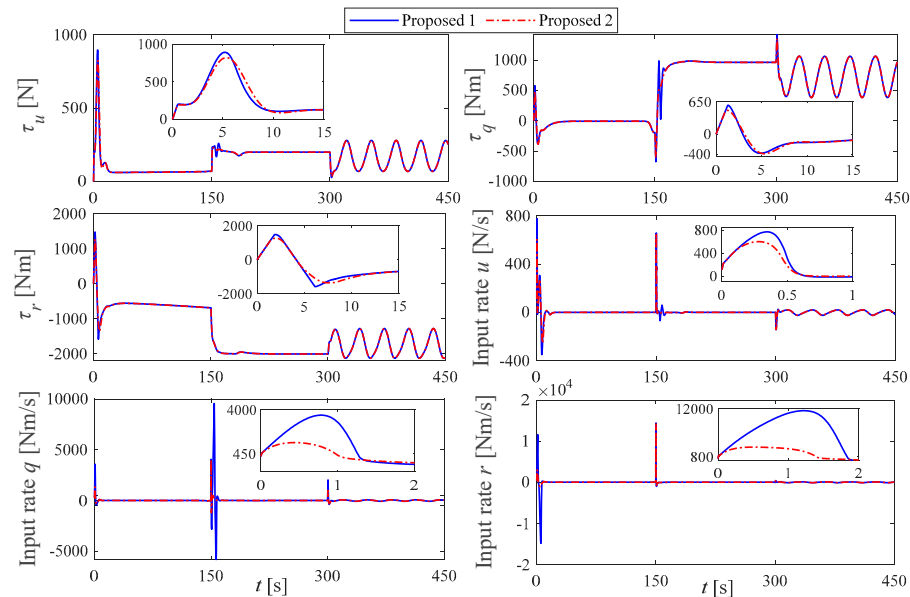


Figure 11. Control inputs for tighter constraints on input rates in Scenario 3.

6. Conclusions

A robust adaptive finite-time controller is presented using a novel disturbance observer-based backstepping control for 3D path-following of an underactuated AUV exposed to parameter uncertainties, external disturbances, and input magnitude/rate saturations. The path-following error system is built based on the virtual guidance method. For this system, a control architecture with a two-layer structure is proposed. A finite-time BSC-based kinematic controller ensures that the path-following errors converge to a small region around the origin within a finite time. Then, the dynamic layer is designed using a finite-time BSC equipped with a disturbance observer, in which the velocity commands from the kinematic layer are applied as the reference inputs. The lumped uncertainties are compensated by the fixed-time integral sliding mode disturbance observer, where an adaptive law eliminates the need to know the upper bound of the lumped uncertainty rate. The stability analysis of the cascaded closed-loop system is performed via the Lyapunov stability theorem, which verifies that the path-following errors converge to an arbitrarily small region around zero within a finite time. The effectiveness of the control scheme in 3D path-following is studied with numerical simulations under different working conditions. Compared to the traditional BSC-based methods, the presented controller is characterized by smoother control signals while ensuring excellent system robustness. Although the proposed control law is specifically designed for the path-following of underactuated AUVs, it can be easily adapted for other autonomous vehicles and robotic systems.

Given the unknown initial states of AUVs, the convergence time may be prolonged for initial errors far from the origin. Future work will be devoted to designing a fixed-

time control law and evaluating the control performance in terms of convergence rate and robustness.

Author Contributions: Conceptualization, M.E.; methodology, M.E. and M.L.; software, M.E.; validation, M.E. and M.L.; formal analysis, M.E. and M.L.; investigation, M.L.; writing—original draft preparation, M.E.; writing—review and editing, M.L.; supervision, M.L. All authors have read and agreed to the published version of the manuscript.

Funding: This research received no external funding.

Data Availability Statement: The data presented in this study are available on request from the first author. The data are not publicly available due to privacy.

Conflicts of Interest: The authors declare no conflicts of interest.

References

- Zhang, J.; Xiang, X.; Lapierre, L.; Zhang, Q.; Li, W. Approach-angle-based three-dimensional indirect adaptive fuzzy path following of under-actuated AUV with input saturation. *Appl. Ocean Res.* **2021**, *107*, 102486. [[CrossRef](#)]
- Yu, C.; Xiang, X.; Lapierre, L.; Zhang, Q. Nonlinear guidance and fuzzy control for three-dimensional path following of an underactuated autonomous underwater vehicle. *Ocean Eng.* **2017**, *146*, 457–467. [[CrossRef](#)]
- Hung, N.; Rego, F.; Quintas, J.; Cruz, J.; Jacinto, M.; Souto, D.; Potes, A.; Sebastiao, L.; Pascoal, A. A review of path following control strategies for autonomous robotic vehicles: Theory, simulations, and experiments. *J. Field Robot.* **2023**, *40*, 747–779. [[CrossRef](#)]
- Liang, X.; Qu, X.; Hou, Y.; Zhang, J. Three-dimensional path following control of underactuated autonomous underwater vehicle based on damping backstepping. *Int. J. Adv. Robot. Syst.* **2017**, *14*, 1–9. [[CrossRef](#)]
- Du, P.; Yang, W.; Wang, Y.; Hu, R.; Chen, Y.; Huang, S. A novel adaptive backstepping sliding mode control for a lightweight autonomous underwater vehicle with input saturation. *Ocean Eng.* **2022**, *263*, 112362. [[CrossRef](#)]
- Guo, C.; Han, Y.; Qin, J.; Yu, H. Spatial Path-Following Control of Underactuated AUV With Multiple Uncertainties and Input Saturation. *IEEE Access* **2019**, *7*, 98014–98022. [[CrossRef](#)]
- Miao, J.; Wang, S.; Zhao, Z.; Li, Y.; Tomovic, M.M. Spatial curvilinear path following control of underactuated auv with multiple uncertainties. *ISA Trans.* **2017**, *67*, 107–130. [[CrossRef](#)] [[PubMed](#)]
- Liu, S.; Liu, Y.; Wang, N. Nonlinear disturbance observer-based backstepping finite-time sliding mode tracking control of underwater vehicles with system uncertainties and external disturbances. *Nonlinear Dyn.* **2017**, *88*, 465–476. [[CrossRef](#)]
- Guerrero, J.; Torres, J.; Creuze, V.; Chemori, A. Adaptive disturbance observer for trajectory tracking control of underwater vehicles. *Ocean Eng.* **2020**, *200*, 107080. [[CrossRef](#)]
- Thanh, P.; Tam, P.; Anh, H. A new approach for three-dimensional trajectory tracking control of under-actuated AUVs with model uncertainties. *Ocean Eng.* **2021**, *228*, 108951. [[CrossRef](#)]
- Zhang, Y.; Liu, J.; Yu, J. Adaptive asymptotic tracking control for autonomous underwater vehicles with non-vanishing uncertainties and input saturation. *Ocean Eng.* **2023**, *276*, 114280. [[CrossRef](#)]
- Liang, X.; Qu, X.; Wan, L.; Ma, Q. Three-Dimensional Path Following of an Underactuated AUV Based on Fuzzy Backstepping Sliding Mode Control. *Int. J. Fuzzy Syst.* **2018**, *20*, 640–649. [[CrossRef](#)]
- Zhang, T.; Lei, M.; Jiang, D.; Li, Y.; Pang, S. Output-feedback path-following control of underactuated AUVs via singular perturbation and interconnected-system technique. *ISA Trans.* **2024**, *151*, 103–116. [[CrossRef](#)] [[PubMed](#)]
- Zhang, G.; Huang, H.; Qin, H.; Wan, L.; Li, Y.-M.; Cao, J.; Su, Y.-M. A novel adaptive second order sliding mode path following control for a portable AUV. *Ocean Eng.* **2018**, *151*, 82–92. [[CrossRef](#)]
- Li, B.; Gao, X.; Huang, H.; Yang, H. Improved adaptive twisting sliding mode control for trajectory tracking of an AUV subject to uncertainties. *Ocean Eng.* **2024**, *297*, 116204. [[CrossRef](#)]
- An, S.; Wang, L.; He, Y. Robust fixed-time tracking control for underactuated AUVs based on fixed-time disturbance observer. *Ocean Eng.* **2022**, *266 Pt 1*, 112567. [[CrossRef](#)]
- Cui, R.; Zhang, X.; Cui, D. Adaptive sliding-mode attitude control for autonomous underwater vehicles with input nonlinearities. *Ocean. Eng.* **2016**, *123*, 45–54. [[CrossRef](#)]
- Cui, R.; Chen, L.; Yang, C.; Chen, M. Extended State Observer-Based Integral Sliding Mode Control for an Underwater Robot With Unknown Disturbances and Uncertain Nonlinearities. *IEEE Trans. Ind. Electron.* **2017**, *64*, 6785–6795. [[CrossRef](#)]
- Xu, J.; Wang, M.; Qiao, L. Dynamical sliding mode control for the trajectory tracking of underactuated unmanned underwater vehicles. *Ocean Eng.* **2015**, *105*, 54–63. [[CrossRef](#)]

20. Lakhekar, G.; Waghmare, L.; Jadhav, P.; Roy, R. Robust Diving Motion Control of an Autonomous Underwater Vehicle Using Adaptive Neuro-Fuzzy Sliding Mode Technique. *IEEE Access* **2020**, *8*, 109891–109904. [[CrossRef](#)]
21. Zhang, X.; Yao, B.; Lian, L.; Mao, Z. Adaptive neural network sliding mode tracking control with prescribed performance for an underwater glider under input saturation. *Ocean Eng.* **2024**, *307*, 118150. [[CrossRef](#)]
22. He, L.; Zhang, Y.; Li, S.; Li, B.; Yuan, Z. Three-Dimensional Path Following Control for Underactuated AUV Based on Ocean Current Observer. *Drones* **2024**, *8*, 672. [[CrossRef](#)]
23. Fossen, T.; Aguiar, A.P. A uniform semiglobal exponential stable adaptive line-of-sight (ALOS) guidance law for 3-D path following. *Automatica* **2024**, *163*, 111556. [[CrossRef](#)]
24. Kim, M.H.; Lee, D.; Kim, D.W. Three-dimensional path-following control of nonlinear autonomous underwater vehicles with actuator saturation. *Ocean Eng.* **2025**, *317*, 119966. [[CrossRef](#)]
25. Shen, K.; Yu, C.; Guo, Y.; Zhong, Y.; Cao, J.; Xiang, X.; Lian, L. Hybrid-tracked finite-time path following control of underactuated underwater vehicles with 6-DOF. *Ocean Eng.* **2024**, *312 Pt 1*, 119023. [[CrossRef](#)]
26. Li, J.; Xia, Y.; Xu, G.; Guo, Z.; Han, H.; Wu, Z.; Xu, K. Enhanced three-dimensional trajectory tracking control for AUVs in variable operating conditions using FMPC-FTTSMC. *Ocean Eng.* **2024**, *310 Pt 2*, 118805. [[CrossRef](#)]
27. Hou, Y.; Wang, H.; Wei, Y.; Ho-Ching Iu, H.; Fernando, T. Robust adaptive finite-time tracking control for Intervention-AUV with input saturation and output constraints using high-order control barrier function. *Ocean Eng.* **2023**, *268*, 113219. [[CrossRef](#)]
28. Liu, H.; Zhuo, J.; Tian, X.; Mai, Q. Finite-time self-structuring neural network trajectory tracking control of underactuated autonomous underwater vehicles. *Ocean Eng.* **2023**, *268*, 113450. [[CrossRef](#)]
29. Thuyen, N.A.; Thanh, P.; Anh, H. Adaptive finite-time leader-follower formation control for multiple AUVs regarding uncertain dynamics and disturbances. *Ocean Eng.* **2023**, *269*, 113503. [[CrossRef](#)]
30. Ji, S.; Thai, B.; Yoo, S.; Youn, W. A novel fuzzy adaptive finite-time extended state observer based robust control for an autonomous underwater vehicle subject to external disturbances and measurement noises. *Ocean Eng.* **2025**, *318*, 120141. [[CrossRef](#)]
31. An, S.; Wang, X.; Wang, L.; He, Y. Observer based fixed-time integral sliding mode tracking control for underactuated AUVs via an event-triggered mechanism. *Ocean Eng.* **2023**, *284*, 115158. [[CrossRef](#)]
32. Zheng, J.; Song, L.; Liu, L.; Yu, W.; Chen, C. Fixed-time sliding mode tracking control for autonomous underwater vehicles. *Appl. Ocean Res.* **2021**, *117*, 102928. [[CrossRef](#)]
33. Ellenrieder, K. Stable Backstepping Control of Marine Vehicles with Actuator Rate Limits and Saturation. *IFAC-PapersOnLine* **2018**, *51*, 262–267. [[CrossRef](#)]
34. Liu, Y.; Liu, J.; Wang, Q.; Yu, J. Adaptive Command Filtered Backstepping Tracking Control for AUVs Considering Model Uncertainties and Input Saturation. *IEEE Trans. Circuits Syst. II Express Briefs* **2023**, *70*, 1475–1479. [[CrossRef](#)]
35. Meng, C.; Zhang, W.; Du, X. Finite-time extended state observer based collision-free leaderless formation control of multiple AUVs via event-triggered control. *Ocean Eng.* **2023**, *268*, 113605. [[CrossRef](#)]
36. Sun, P.; Zho, B.; Zuo, Z.; Basin, M. Vision-based finite-time uncooperative target tracking for UAV subject to actuator saturation. *Automatica* **2021**, *130*, 109708. [[CrossRef](#)]
37. Ebrahimpour, M.; Lungu, M.; Kakavand, M. Antisaturation fixed-time backstepping fuzzy integral sliding mode control for automatic landing of fixed-wing unmanned aerial vehicles. *J. Frank. Inst.* **2024**, *361*, 107185. [[CrossRef](#)]
38. Wang, F.; Lai, G. Fixed-time control design for nonlinear uncertain systems via adaptive method. *Syst Control Lett.* **2020**, *140*, 104704. [[CrossRef](#)]
39. Choukri Lamraoui, H.; Qidan, Z. Path following control of fully-actuated autonomous underwater vehicle in presence of fast-varying disturbances. *Appl. Ocean Res.* **2019**, *86*, 40–46. [[CrossRef](#)]

Disclaimer/Publisher's Note: The statements, opinions and data contained in all publications are solely those of the individual author(s) and contributor(s) and not of MDPI and/or the editor(s). MDPI and/or the editor(s) disclaim responsibility for any injury to people or property resulting from any ideas, methods, instructions or products referred to in the content.